Biomedical Optics EXPRESS

Synthesis and characterization of biocompatible nanodiamond-silk hybrid material

Asma Khalid,[1,*] Rebecca Lodin,[2] Peter Domachuk,[2] Hu Tao,[3] Jodie E. Moreau,[3] David L. Kaplan,[3] Fiorenzo G. Omenetto,[3,4] Brant C. Gibson[5,1] and Snjezana Tomljenovic-Hanic[1]

[1] *School of Physics, University of Melbourne, Parkville, VIC 3010, Australia*
[2] *School of Physics, University of Sydney, Camperdown, NSW 2006, Australia*
[3]*Department of Biomedical Engineering, Tufts University, Medford, Massachusetts 02155, USA*
[4]*Department of Physics, Tufts University, Medford, Massachusetts 02155, USA*
[5]*present address: Applied Physics, School of Applied Sciences, RMIT University, Melbourne 3001, Australia*
[*]*asmak@student.unimelb.edu.au*

Abstract: A new hybrid material consisting of nanodiamonds (NDs) and silk has been synthesized and investigated. NDs can contain bright fluorescence centers, important for bioprobes to image biological structures at the nanoscale and silk provides a transparent, robust matrix for these nanoparticles *in-vivo* or *in-vitro*. The ND-silk hybrid films were determined to be highly transparent in the visible to near infrared wavelength range. The NDs embedded in silk exhibited significant enhancement of emission relative to air, correlating with theoretical predictions. Furthermore, animal toxicity tests confirmed ND-silk films to be non-toxic in an *in-vivo* mice model.

OCIS codes: (160.4236) Nanomaterials; (180.1790) Confocal microscopy; (300.2530) Fluorescence, laser-induced.

References and links

1. D. Ho, *Nanodiamonds applications in biology and nanoscale medicine* (Springer Link, New York, USA, 2010), Chap. 6.
2. X. Zhang, W. Hu, J. Li, L. Tao, and Y. A. Wei, "Comparative study of cellular uptake and cytotoxicity of multi-walled carbon nanotubes, graphene oxide and nanodiamond," Toxicol. Rev. **1**, 62–68 (2012).
3. E. K. Chow, X. Q. Zhang, M. Chen, R. Lam, E. Robinson, H. Huang, D. Schaffer, E. Osawa, A. Goga, and D. Ho, "Nanodiamond therapeutic delivery agents mediate enhanced chemoresistant tumor treatment," Sci. Transl. Med. **3**(73), 73ra21 (2011).
4. J. Tisler, R. Reuter, A. Lämmle, F. Jelezko, G. Balasubramanian, P. R. Hemmer, F. Reinhard, and J. Wrachtrup, "Highly efficient FRET from a single nitrogen-vacancy center in nanodiamonds to a single organic molecule," ACS Nano **5**(10), 7893–7898 (2011).
5. V. N. Mochalin, O. Shenderova, D. Ho, and Y. Gogotsi, "The properties and applications of nanodiamonds," Nat. Nanotechnol. **7**(1), 11–23 (2011).
6. A. S. Barnard, "Diamond standard in diagnostics: nanodiamond biolabels make their mark," Analyst (Lond.) **134**(9), 1751–1764 (2009).
7. P. Alivisatos, "The Use of nanocrystals in biological detection," Nat. Biotechnol. **22**(1), 47–52 (2004).
8. A. M. Derfus, W. C. W. Chan, and S. N. Bhatia, "Probing the cytotoxicity of semiconductor quantum dots," Nano Lett. **4**(1), 11–18 (2004).
9. A. Stacey, D. A. Simpson, T. J. Karle, B. C. Gibson, V. M. Acosta, Z. Huang, K.-M. Fu, C. C. Santori, R. G. Beausoleil, L. P. McGuinness, K. Ganesan, S. Tomljenovic-Hanic, A. D. Greentree, and S. Prawer, "Near-surface spectrally stable nitrogen vacancy centers engineered in single crystal diamond," Adv. Mater. **24**(25), 3333–3338 (2012).
10. Y. Y. Hui, C.-L. Cheng, and H.-C. Chang, "Nanodiamonds for optical bioimaging," J. Phys. D Appl. Phys. **43**(37), 374021 (2010).
11. R. A. Shimkunas, E. Robinson, R. Lam, S. Lu, X. Xu, X.-Q. Zhang, H. Huang, E. Osawa, and D. Ho, "Nanodiamond-insulin complexes as pH-dependent protein delivery vehicles," Biomaterials **30**(29), 5720–5728 (2009).
12. M. Chen, X.-Q. Zhang, H. B. R. Lam, E. K. Chow, and D. Ho, "Nanodiamond vectors functionalized with polyethylenimine for siRNA delivery," J. Phys. Chem. Lett. **1**(21), 3167–3171 (2010).

#197546 - $15.00 USD Received 17 Sep 2013; revised 27 Nov 2013; accepted 12 Dec 2013; published 27 Jan 2014

13. H. B. Man and D. Ho, "Diamond as a nanomedical agent for versatile applications in drug delivery, imaging, and sensing," Phys. Status Solidi A. **209**(9), 1609–1618 (2012).
14. R. V. Lewis, "Spider silk: ancient ideas for new biomaterials," Chem. Rev. **106**(9), 3762–3774 (2006).
15. D.-H. Kim, Y.-S. Kim, J. Amsden, B. Panilaitis, D. L. Kaplan, F. G. Omenetto, M. R. Zakin, and J. A. Rogers, "Silicon electronics on silk as a path to bioresorbable, implantable devices," Appl. Phys. Lett. **95**(13), 133701 (2009).
16. C. Vepari and D. L. Kaplan, "Silk as a Biomaterial," Prog. Polym. Sci. **32**(8-9), 991–1007 (2007).
17. S. T. Parker, P. Domachuk, J. Amsden, J. Bressner, J. A. Lewis, D. L. Kaplan, and F. G. Omenetto, "Biocompatible silk printed optical waveguides," Adv. Mater. **21**(23), 2411–2415 (2009).
18. A. B. Mathur and V. Gupta, "Silk fibroin-derived nanoparticles for biomedical applications," Nanomedicine (Lond) **5**(5), 807–820 (2010).
19. E. Kharlampieva, V. Kozlovskaya, B. Wallet, V. V. Shevchenko, R. R. Naik, R. Vaia, D. L. Kaplan, and V. V. Tsukruk, "Co-cross-linking silk matrices with silica nanostructures for robust ultrathin nanocomposites," ACS Nano **4**(12), 7053–7063 (2010).
20. K. Tsioris, G. E. Tilburey, A. R. Murphy, P. Domachuk, D. L. Kaplan, and F. G. Omenetto, "Functionalized-silk-based active optofluidic devices," Adv. Funct. Mater. **20**(7), 1083–1089 (2010).
21. E. M. Pritchard, T. Valentin, B. Panilaitis, F. G. Omenetto, and D. L. Kaplan, "Antibiotic-releasing silk biomaterials for infection prevention and treatment," Adv. Funct. Mater. **23**(7), 854–861 (2013).
22. E. Ampem-Lassen, D. A. Simpson, B. C. Gibson, S. Trpkovski, F. M. Hossain, S. T. Huntington, K. Ganesan, L. C. L. Hollenberg, and S. Prawer, "Nano-manipulation of diamond-based single photon sources," Opt. Express **17**(14), 11287–11293 (2009).
23. R. H. Brown and R. Q. Twiss, "Correlation between photons in two coherent beams of light," Nature **177**(4497), 27–29 (1956).
24. A. Beveratos, R. Brouri, T. Gacoin, J.-P. Poizat, and P. Grangier, "Nonclassical radiation from diamond nanocrystals," Phys. Rev. A **64**(6), 061802 (2001).
25. P. Domachuk, H. Perry, J. J. Amsden, D. L. Kaplan, and F. G. Omenetto, "Bioactive "self-sensing" optical systems," Appl. Phys. Lett. **95**(25), 253702 (2009).
26. F. G. Omenetto and D. L. Kaplan, "A new route for silk," Nat. Photonics **2**(11), 641–643 (2008).
27. F. A. Inam, T. Gaebel, C. Bradac, L. Stewart, M. J. Withford, J. M. Dawes, J. R. Rabeau, and M. J. Steel, "Modification of spontaneous emission from nanodiamond colour centers on a structured surface," New J. Phys. **13**(7), 073012 (2011).
28. W. Lukosz and R. E. Kunz, "Fluorescence lifetime of magnetic and electric dipoles near a dielectric interface," Opt. Commun. **20**(2), 195–199 (1977).
29. H. Chew, "Radiation and lifetimes of atoms inside dielectric particles," Phys. Rev. A **38**(7), 3410–3416 (1988).
30. W. Lukosz and R. E. Kunz, "Light-emission by magnetic and electric dipoles close to a plane interface. I. Total radiated power," J. Opt. Soc. Am. **67**(12), 1607–1615 (1977).
31. W. Lucosz and R. E. Kunz, "Light-emission by magnetic and electric dipoles close to a plane interface II Radiation patterns of perpendicular oriented dipoles," J. Opt. Soc. Am. **67**(12), 1615–1619 (1977).
32. L. Novotny and B. Hercht, *Principles of Nano-Optics* (Cambridge University press, Cambridge, UK, 2006), Chap. 10.
33. H. Tao, D. L. Kaplan, and F. G. Omenetto, "Silk materials-a road to sustainable high technology," Adv. Mater. **24**(21), 2824–2837 (2012).
34. B. D. Lawrence, M. Cronin-Golomb, I. Georgakoudi, D. L. Kaplan, and F. G. Omenetto, "Bioactive silk protein biomaterial systems for optical devices," Biomacromolecules **9**(4), 1214–1220 (2008).

1. Introduction

Nanobiotechnology is a rapidly emerging field which promises the development of new types of diagnostic and therapeutic techniques for biomedicine. The technologies based on the utilization of nanoparticles are particularly expected to improve our knowledge of biological systems and mechanisms at the molecular and cellular level [1]. In this regard, fluorescent nanodiamonds (NDs) are increasingly studied due to their non-cytotoxicity [2,3] and stable emission at room temperature [4].The negatively charged nitrogen vacancy (NV^-) center [4,5] is one of a number of color centers in diamond which is an exceptionally photostable single photon emitter at room temperature [4]. The NV^- center consists of a substitutional nitrogen atom adjacent to a vacancy surrounded by a carbon lattice, as shown to the inset of Fig. 1(a). The center emits red fluorescence at a zero phonon line ($\lambda \approx 637$ nm) and a phonon side band ($\lambda \approx 650$-850 nm) when excited with a green laser ($\lambda \approx 532$ nm), as shown by the emission spectrum of Fig. 1(b), taken at room temperature. Optical excitation and sensing with an NV^- center occurs in the wavelength range which does not interfere with cellular processes [6].

#197546 - $15.00 USD Received 17 Sep 2013; revised 27 Nov 2013; accepted 12 Dec 2013; published 27 Jan 2014

The NV^- center in diamond circumvents the limitations of organic dyes, fluorescent proteins and quantum dots (QDs) [1]. Photo-bleaching is the major issue in the case of organic fluorophores and fluorescent proteins [7] hampering their use in long term monitoring, whereas QDs, despite of having high levels of brightness and photostability, possess inherent toxicity, hindering their *in-vivo* applications [1,8]. The photostability of the NV^- center [9] combined with the biocompatibility of diamond makes NDs highly suitable for long-term imaging and monitoring in cellular environments [10]. Due to these characteristics, NDs have been investigated in nanomedicine in the areas of drug delivery (for cancer therapy [3], protein [11] and gene [12] delivery), targeted bioimaging (fluorescence monitoring) and biosensing [13].

On the other hand, silk, a natural protein fiber has been used in biomedicine for centuries [14] due to its non-inflammatory response. Silk fibroin derived films are highly flexible, biodegradable and biocompatible *in-vitro* and *in-vivo* [15,16]. These properties make silk an outstanding material and an excellent substrate for the fabrication of implantable and degradable bio-optical devices [17]. Moreover, silk's ability to be functionalized with biochemistries on one hand and with optical components on the other hand suggests that silk forms an excellent underlying substance for fabricating biomedical materials and biomolecular sensing devices [18–20]. Silk films are particularly good for implants and biocompatible substrates (for electronic devices) as they have the ability to establish conformal contact with the curved surfaces of the tissues and organs [15].

So far, the studies on both NDs and silk standalone but combining these two materials will immensely magnify the functionalities of each of them. The optical component of silk is of extraordinary importance to NDs. Delivering and collecting light with flexible and biocompatible silk-based optical elements is crucial for future imaging and sensing applications of NDs. It is important to mention here that silk fibroin films possess high transparency in the emission wavelength range of the NV^- center [19]. The transmission spectrum of silk fibroin is presented with the black line in Fig. 1(b), which shows high optical transmission (≈90%) through silk in the wavelength range of NV^- emission. On the other hand, the addition of biocompatible dopants such as NDs increases the optical probing and chemical interaction regions of silk. Inorganic fluorescent dopants [18] have been integrated in silk fibroin matrices, but it is important to strive to maintain maximum biocompatibility of the components that are included in silk. Due to this reason, NDs are the most suitable candidates to use in conjugation with silk as they possess inherent biocompatibility, non-toxicity [6], and stable luminescence [4]. With flexible and biocompatible silk-based optical elements, NDs would make excellent optical components for delivering and collecting light for the future biosensing applications.

Few of the many applications that may result from the combination of these two biocompatible materials are targeted drug delivery using a range of ND-silk structures (from injectable silk encapsulated NDs to implantable ND-silk films), monitored antibiotic release in an infectious area with drug loaded ND-silk films in addition to biosensing at the nanoscale. With tuneable degradability, ND-silk film implants can be used for a controlled release of bioactive antibiotics and infection prevention at the target site [21].

Here, we show the composition and characterization of hybrid biocompatible ND-silk films. A schematic of the hybrid film including the method of optical characterization is shown in Fig. 1(a). The new hybrid film exhibits enhanced emission of optical centers by integrating features from both the bioderived silk fibers and fluorescent NDs.

2. Results and discussion

First the optical transmission of silk was examined with and without NDs. Then, the change in the emission properties of NDs embedded in silk relative to air was studied. A theoretical model was used to explain the experimentally observed enhanced emission from NDs. Lastly, the non-toxicity of the ND-doped silk films was evaluated through an *in-vivo* model.

#197546 - $15.00 USD Received 17 Sep 2013; revised 27 Nov 2013; accepted 12 Dec 2013; published 27 Jan 2014

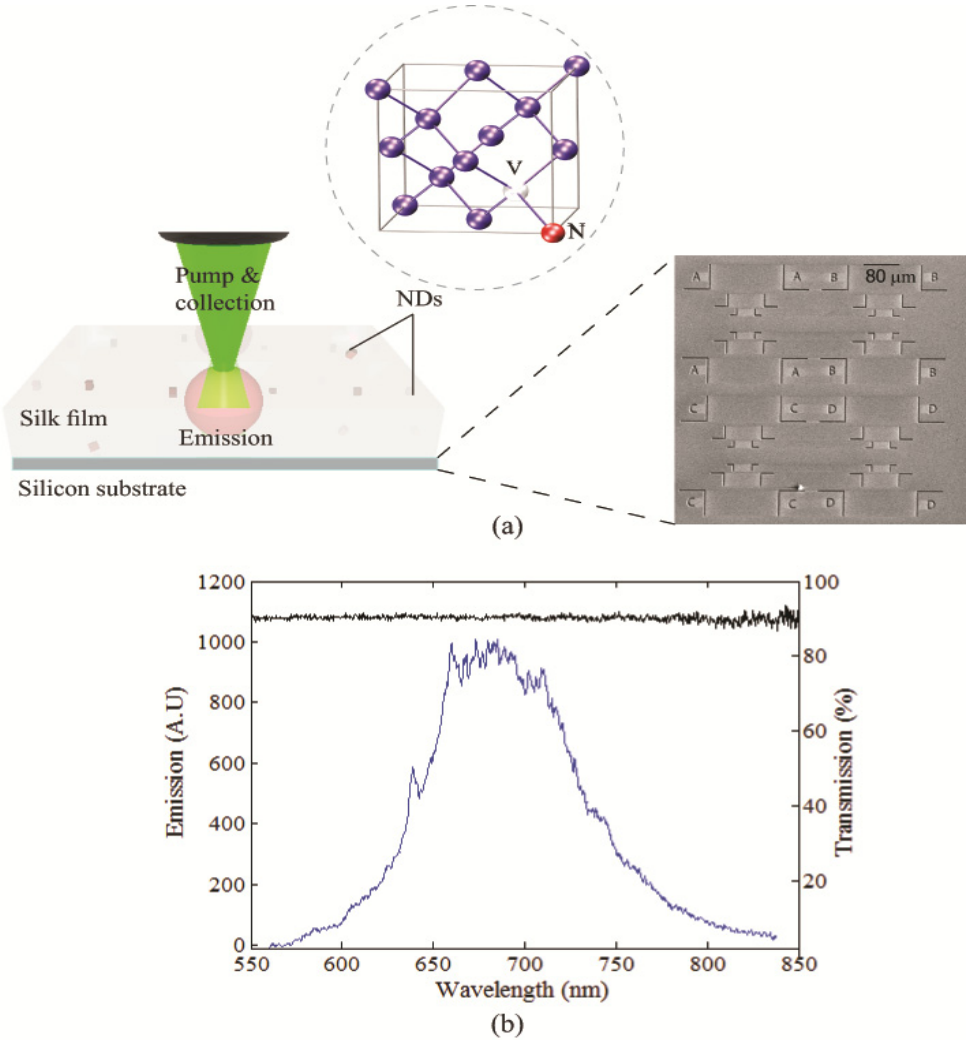

Fig. 1. (a) Schematic representation of a silk-coated ND (on silicon substrate) fluorescing in red (a characteristic of NV^- center), when pumped with a green laser (532 nm). The crystallographic model of the NV^- center in diamond is shown in the inset, consisting of a substitutional nitrogen atom adjacent to a vacancy [9]. Scanning electron microscopy (SEM) image of the marked silicon substrate used to identify the NDs after silk coating is shown to the right. (b) Emission spectrum of a single NV^- center in ND (blue) at room temperature with a visible zero phonon line at 637 nm and transmission spectrum of silk (black) showing a high (≈90%) transmission in the wavelength range of interest. The scale on left shows the intensity of the spectrum in arbitrary units, while that on right shows the transmission percentage.

2.1 Transmission properties

The spectral properties of silk films were investigated with and without NDs. An aqueous silk solution containing 6% by weight of silk fibroin was used. Commercially available NDs (with an average size of 45 nm) in an aqueous solution with a concentration of 0.4 mg/mL were mixed to the silk solution. Free standing silk films, (with and without NDs) were prepared with an average thickness of ≈50 µm shown in the inset of Fig. 2. Both films were found to be highly transparent with transmission (≈80-90%) across most of the visible spectrum as shown in Fig. 2. However, small losses in transmission (< 5%) can be seen for the NDs doped silk film, which can be attributed to the scattering of light by NDs.

#197546 - $15.00 USD Received 17 Sep 2013; revised 27 Nov 2013; accepted 12 Dec 2013; published 27 Jan 2014

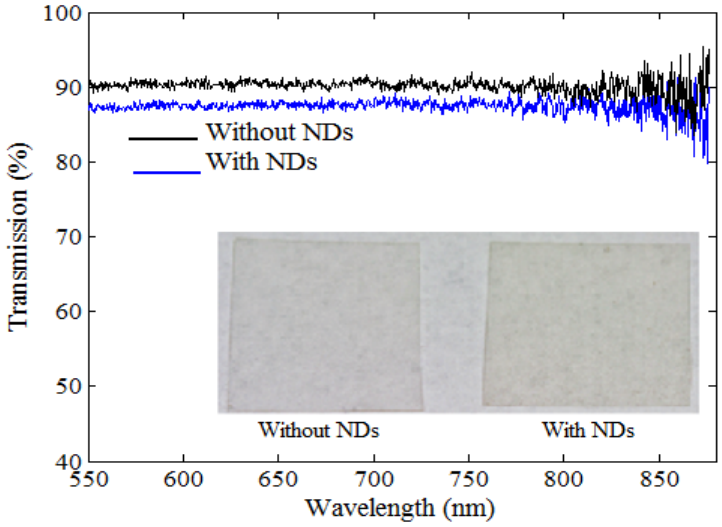

Fig. 2. Transmission spectra of silk without (black line) and with NDs (blue line). Inset shows the free standing silk only (left) and NDs mixed with silk (right) film.

2.2 Emission measurements

After determining the transmission properties, the next step was to evaluate the change in the optical emission properties of NDs embedded in silk. The ND solution (2 mg/mL) was drop-cast on a marked silicon substrate (5 mm x 5 mm). An SEM image (300 µm × 300 µm) of the substrate with the reference markers [22] is shown to the right of Fig. 1(a). This provided the ability to address the same NDs before and after silk coating. The schematic of this hybrid film and its optical characterization are presented to the left of the same figure. Scanning confocal fluorescence maps were taken with an excitation power of 600 µW at a wavelength $\lambda = 532$ nm and fluorescence collected in a spectral window of 650 nm to 750 nm.

A total of eleven NV^- defect centers with single photon emission were analyzed in this part of experiment. The data from one of these centers prior to coating with silk is presented in Fig. 3.

Figure 3(a) shows a 5 µm × 5 µm confocal map of NV^- fluorescence from NDs on the silicon substrate. The bright fluorescent circular regions in the image correspond to NDs that can contain single or multiple NV^- defects. The presence of a single defect inside a particular ND was confirmed using a Hanbury Brown and Twiss (HBT) single photon antibunching system [23]. Figure 3(b) shows antibunching data from the ND (marked with the cross hair in Fig. 3(a)) exhibiting a characteristic dip at the zero delay time. Its second order correlation function $g^{(2)}(t)$ approaches zero as the time delay approaches zero [24], which signifies antibunching of photons emitted from the labeled ND. The counts for this particle were recorded for 3 minutes as shown by the blue trace of Fig. 4. The background-subtracted average counts were found to be around 20,000 per second.

#197546 - $15.00 USD Received 17 Sep 2013; revised 27 Nov 2013; accepted 12 Dec 2013; published 27 Jan 2014

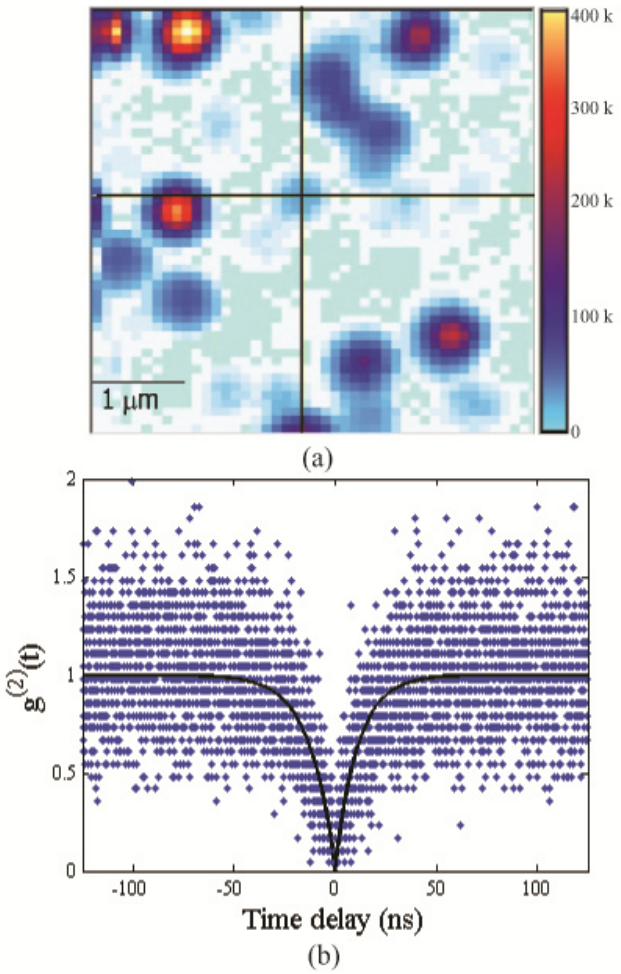

Fig. 3. (a) Scanning confocal fluorescence map of a 5 μm × 5 μm region of the sample before coating with silk. The cross hair specifies a ND containing a single defect center. (b) Photon antibunching plot for the center identified in (a). Black curve is a single exponential fit of the antibunching data [24].

To study the quantitative change in the emission properties of silk-coated NDs, a thin film of silk was coated on top of the NDs positioned on the silicon substrate. Silk processing was carried out using previously published methods [25,26] to yield an aqueous solution of silk fibroin protein, which was then drop-cast on top of NDs/silicon substrate. The solution was left to dry in air until the crystallization of silk formed an optically clear film with thickness ≈850 nm on the top of NDs/silicon substrate.

The silk-coated-NDs film on silicon was again analyzed on the scanning confocal fluorescence microscope. Using reference markers, the same 5 μm × 5 μm region of Fig. 3(a) was located and re-scanned as shown in Fig. 5(a). The same NV^- single center, analyzed before silk coating, was again checked for photon antibunching. Figure 5(b) shows the dip in $g^{(2)}(t)$ function at zero time delay, which confirmed the presence of single NV^- center after silk coating. The counts per second emitted by the center were re-tracked (Fig. 4, red trace) for 3 minutes and plotted against time.

The background-subtracted average counts after silk coating were found to be around 43,000 per second which is 2.2 times higher than the average counts before coating. A

#197546 - $15.00 USD Received 17 Sep 2013; revised 27 Nov 2013; accepted 12 Dec 2013; published 27 Jan 2014

comparison of the emission rates for the same single NV^- center before and after silk coating is shown in Fig. 4.

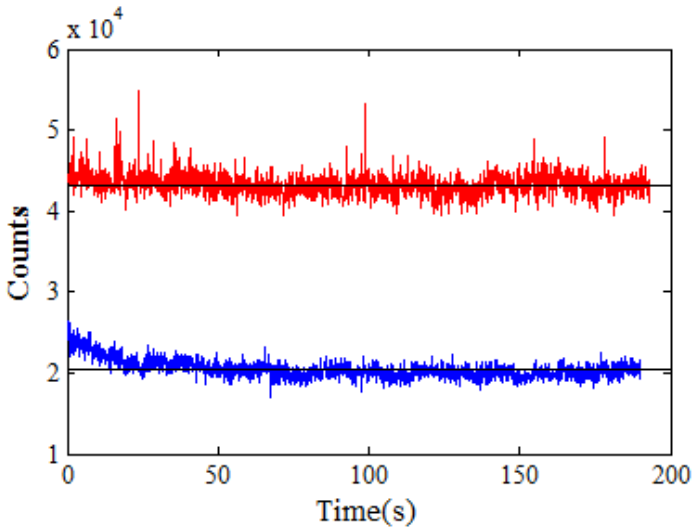

Fig. 4. Background subtracted emission from the NV^- center (blue trace) showing an approximately 2 fold increase in counts after being embedded in silk (red trace). The black lines represent the average counts for the corresponding count rates.

A comparison of the fits of the $g^{(2)}(t)$ data from Fig. 3(b) and Fig. 5(b) was then performed. The decay constants τ_1 and τ_2 for the two curves were calculated (through least squares curve fitting) and used to approximate the life time τ_1 and τ_2 of the center before and after silk coating respectively [24]. Since the emission rate Γ is inversely proportional to the lifetime i.e., $\Gamma\alpha\ 1/\tau$ [27], hence $\tau_2 \sim (1/2 \times \tau_1)$ for the center showing a 2.2 times emission enhancement. The approximately calculated life time for the center after coating $\tau_2 \approx 4.2$ ns is nearly half of the approximated life time before coating $\tau_1 \approx 10.0$ ns, which can also be observed through the difference in the $g^{(2)}(t)$ fit of Fig. 5(b).

The process of tracking and re-tracking the same center, recording count rates and antibunching data was repeated for eleven single NV^- centers before and after silk coating. Each of the single centers was found to exhibit an enhanced emission rate after being covered with silk. The enhancement factor was found to vary in a range of 1.6 - 3.8 times. The data for these eleven centers is shown in Table 1, which statistically proves the enhancement effect in silk coated NDs.

A brief discussion of the theoretical model to compute the NDs' emission rate ratio in silk with respect to air is presented here. The excited NV^- center radiating at $\lambda \approx 637$ nm can be approximated by an oscillating electric dipole, trapped inside the ND sphere. The model is based on the mathematical formulation for power radiated by an electric dipole located close to a plane interface [28] and encapsulated inside a spherical nanoparticle [29]. A schematic of the model is shown in Fig. 6(a).

#197546 - $15.00 USD Received 17 Sep 2013; revised 27 Nov 2013; accepted 12 Dec 2013; published 27 Jan 2014

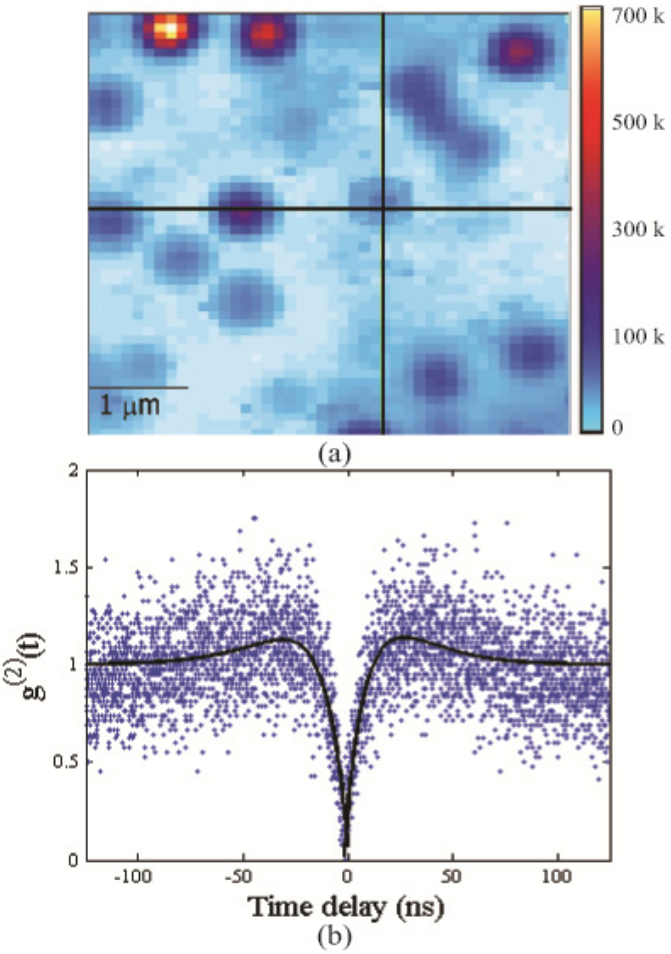

Fig. 5. (a) Scanning confocal fluorescence map of a 5 μm × 5 μm region of the sample after coating with silk. The cross hair specifies the same defect center as shown in Fig. 3. (b) Photon antibunching plot for the center identified in (a). The black curve indicates a double exponential fit of the antibunching data [24].

Table 1. ***Comparison of emission rates from NV⁻ single centers before and after silk coating.***

NV^- center	Average counts/s × 10^3 (NDs in air)	Average counts/s × 10^3 (NDs in silk)	Increase in counts
1	20.4 ± 1.2	43.2 ± 1.4	2.2 ± 0.2
2	61.0 ± 2.1	143.2 ± 9.3	2.3 ± 0.2
3	182.4 ± 2.5	302.7 ± 4.7	1.6 ± 0.1
4	32.3 ± 0.8	70.1 ± 0.7	2.2 ± 0.3
5	31.1 ± 1.5	74.2 ± 7.3	2.4 ± 0.2
6	50.7 ± 2.2	131.3 ± 5.4	2.6 ± 0.1
7	51.1 ± 1.7	153.2 ± 17.9	3.0 ± 0.4
8	77.8 ± 2.1	153.9 ± 7.4	1.9 ± 0.1
9	61.3 ± 1.8	233.3 ± 12.5	3.8 ± 0.2
10	43.6 ± 1.9	141.9 ± 11.9	3.2 ± 0.3
11	70.1 ± 1.6	140.9 ± 9.3	2.0 ± 0.1

The NV^- is trapped inside the diamond nanoparticle with a high refractive index (n_d = 2.4 at λ = 637 nm) and in close proximity to the ND/Si interface i.e., $z_0 = \lambda$. The power radiated is significantly different from that radiated in free space or air when such a dipole is captured

#197546 - $15.00 USD Received 17 Sep 2013; revised 27 Nov 2013; accepted 12 Dec 2013; published 27 Jan 2014

inside a spherical particle, close to a planar surface [27–31]. Here z_0 is the dipole's distance from the ND/Si interface and the dipole is assumed to be located in the center of the ND. In this way, z_0 also defines the approximate sub-wavelength size of the ND containing the NV^- center. The encapsulating ND is surrounded by either air (before coating) or silk (n_s = 1.54). The refractive index of the medium to which NV^- radiates (air or silk) is n_1 (n_1 = 1.0 or 1.54) and n_2 is the refractive index of silicon substrate (n_2 = 3.875). Both media are assumed to be isotropic. The dipole is radiating into an upper and a lower space, where the lower space (substrate) is optically denser. The radiated power of the dipole in the upper space, air or silk, is calculated [32].

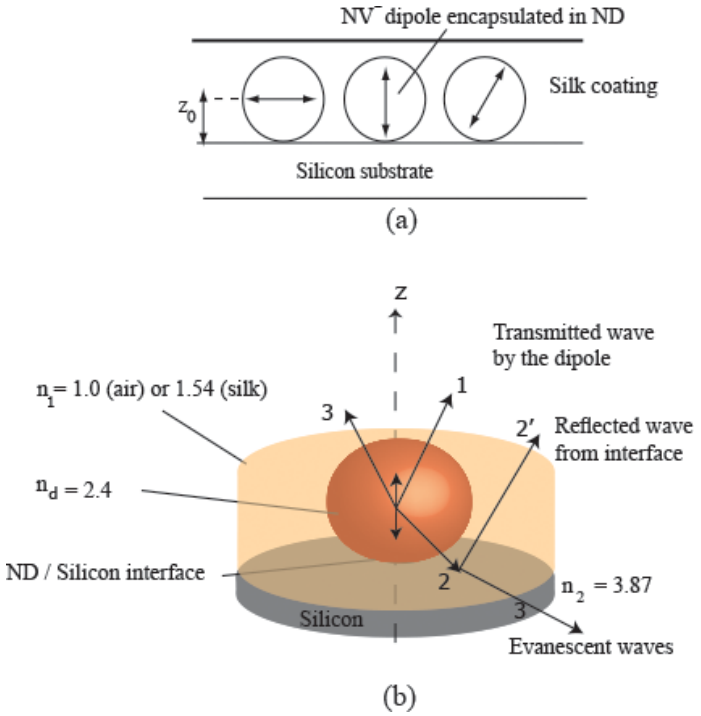

Fig. 6. (a) A schematic of the silk-coated-NDs on the silicon substrate. (b) Radiating NV^- dipole encapsulated in ND, embedded in medium 1 (air/ silk) and lying close to the silicon interface medium 2 (silicon). Interference between the emitted plane wave 1 and the partly reflected wave 2' is shown, which in addition to the reflected evanescent wave contributes to the radiated power.

Evanescent waves are emitted by the dipole as the relative refractive index $n \equiv n_2/n_d$ is larger than unity. These waves are reflected from ND/Si interface and are converted to plane waves when encounter a dielectric medium (air or silk) on top [32]. The evanescent waves provide an additional channel for the dipole to radiate its power into and their contribution causes a significant rise of power for small values of z_0. In addition, the effect of encapsulation of the dipole inside ND also plays its part in the determination of the total power radiated [27, 29] and is mainly dependent on the refractive index ratio n_d/n_1 [29].

The effect of wide field interference in addition to the above two contributions were combined in a single equation to calculate the total radiated power by the NV^- center, trapped in ND and embedded in air or silk. The emission rate from NV^- in ND was normalized with respect to that in bulk diamond ($z \to \infty$). The emission rates R_{ND}^{silk} / R_{bulk} ($n = n_d/1.54$) and R_{ND}^{air} / R_{bulk} ($n = n_d/1.0$) as a function of z were calculated for both orthogonal and parallel polarizations of the dipole. These dipole orientations were defined relative to the silicon's

#197546 - $15.00 USD Received 17 Sep 2013; revised 27 Nov 2013; accepted 12 Dec 2013; published 27 Jan 2014

surface. Finally to compute the enhancement factor e for the emission rates of orthogonal $e^{\perp}$ (solid line) and parallel $e^{\parallel}$ (dashed-dotted) NV^- dipoles, after silk coating, the ratios

$$e^{\perp} = \frac{R^{\perp}silk}{R^{\perp}air} \tag{1a}$$

and

$$e^{\parallel} = \frac{R^{\parallel}silk}{R^{\parallel}air} \tag{1b}$$

were calculated and plotted against ND sizes z as shown in Fig. 7. This theoretically computed enhancement e, in the emission rate with silk coating relative to air, was compared with the corresponding experimentally determined increases in counts, listed in Table 1 for the eleven NV^- centers. The experimental enhancement data was found to be in good agreement with the theoretical modeling showing an increase in the range from 2.8 to 4.9 times for parallel and orthogonal polarizations of the dipoles respectively.

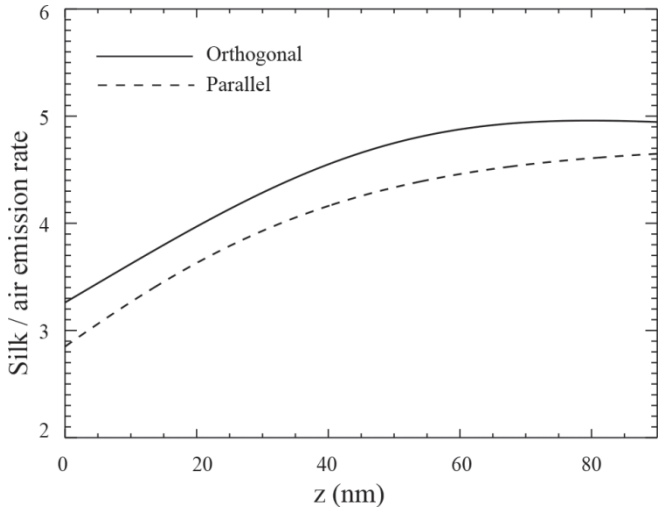

Fig. 7. Emission rate ratio of ND encapsulated NV^- centers covered in silk, relative to air (both on silicon substrate) for orthogonal (solid line) and parallel (dash-dotted) dipole polarizations.

2.3 Toxicity test

Lastly the non-toxicity of ND-silk films was tested *in-vivo* in a mouse model. The ND-silk films were prepared by mixing ND powder with silk fibroin solution (6% by weight) to yield uniform ND-silk solution with a concentration of 0.5 mg/mL. On drop casting, the solution produced optically transparent ND-silk films with a thickness of 50 μm. The films were water annealed to adjust the crystallinity level of the silk fibroin. Two different annealing treatments for partial (1 hour duration) and complete (12 hours duration) annealing were performed to generate two sets of ND-silk film samples. This was done to investigate the effect of annealing on degradability of films after implantation.

The two films were implanted subcutaneously into female Balb/c mice, as shown in Fig. 8(a) and 8(b). The films were retrieved after two weeks to determine device degradation behaviors and the inflammatory response. The fully annealed ND-silk film as shown in Fig. 8(c), degraded completely, nicely encapsulated the embedded NDs and maintained the integrity of the implant after two weeks of implantation. On the other hand, the partially annealed film shown in Fig. 8(d), partly degraded within two weeks of implantation and

#197546 - $15.00 USD Received 17 Sep 2013; revised 27 Nov 2013; accepted 12 Dec 2013; published 27 Jan 2014

released the embedded NDs, which aggregated into localized ND clusters without being circulated and resorbed into the surrounding tissue.

Figure 8(e) shows a histological examination of the tissue surrounding the implant site. The figure reveals the absence of any severed inflammatory response, indicating the implanted devices induced no significant adverse effects to the animals. The experiments were pursued in accordance with Institutional Animal Care and Use Committee (IACUC) approved protocols.

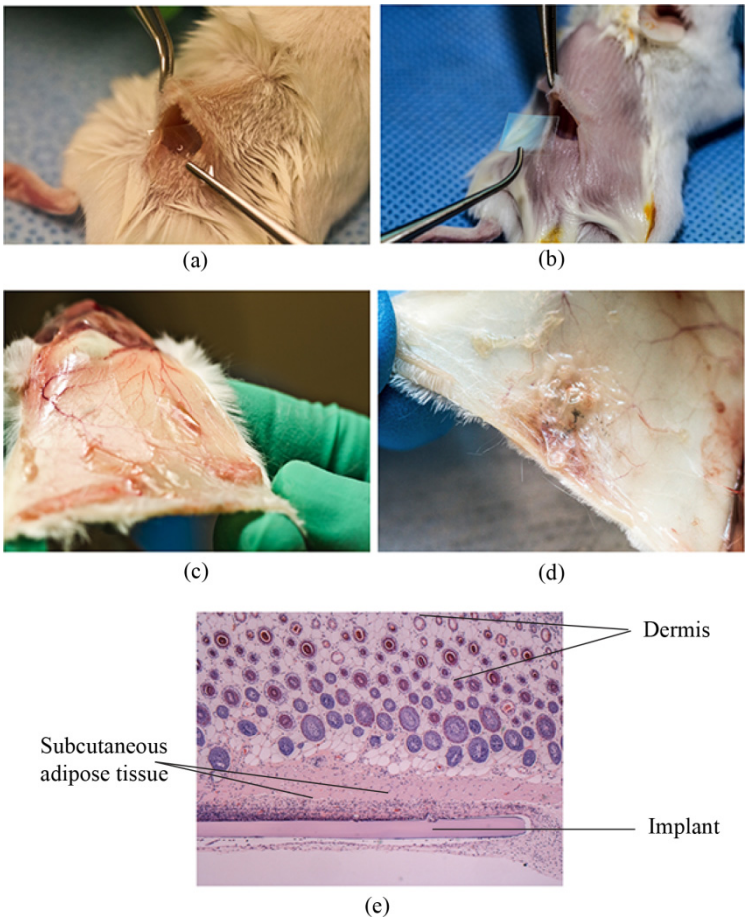

Fig. 8. Animal toxicity test of ND-silk films. Introducing (a) fully and (b) partially annealed films into the animal tissue. Degradation ability and non-inflammatory response of the (c) fully and (d) partially annealed films after two weeks of implantation. (e) A histological image of the examined tissue after implantation, showing no significant adverse effects in the subcutaneous adipose tissue surrounding the ND-silk implant.

3. Conclusions

In this work, films of a new hybrid ND-silk material were synthesized and investigated for their optical properties and non-toxicity *in-vivo*. The ND-silk film was found to be highly transparent in the visible and infrared light range with small scattering losses induced by NDs.

Our results of silk coated NDs showed a significant rise in counts that was 1.6 - 3.8 times higher as compared to the original counts of the ND single emitters without silk coating. This rate of enhancement was found to be in good agreement with the theoretical model. The toxicity test of the ND-silk films *in-vivo* revealed a non-inflammatory response.

#197546 - $15.00 USD Received 17 Sep 2013; revised 27 Nov 2013; accepted 12 Dec 2013; published 27 Jan 2014

Therefore, a new hybrid material that takes advantage of silk's biocompatibility and high transparency combined with the bright and photostable emission characteristics of NDs is capable of extending the range of available bioimaging and sensing techniques. We expect numerous biotechnical and medical applications to emerge as these two extraordinary materials perfectly complement each other.

Future work includes integrating biochemistry into silk and testing the change of emission in ND-silk system upon a binding event. Investigation of more integrated pump and probing sources will be performed so that the device will, eventually, be one integrated chip. The ND-silk hybrid, when used as a sensitive measure of molecular binding, has potential for quick, easy, and disposable drug identification, triage, biochemistry, and molecular medicine.

4. Experimental methods

Commercially available non-detonation NDs (*NaBond*) were used with an average size of 45 nm. These NDs, milled from high temperature high pressure diamond were not irradiated and were used as received. The percentage of NDs containing naturally occurring single NV^- centers is approximately 2% of the NDs which fluoresce.

NDs in aqueous solution with a concentration of 0.4 mg/mL were used for transmission measurements, 2 mg/mL for optical emission characteristics and 0.5 mg/mL of silk solution for the toxicity tests.

Silk solution preparation: The silk fibroin solution was obtained by boiling and de-gumming Bombyx mori cocoons in an alkaline solution of 0.02 M sodium carbonate for 30 minutes. The silk fiber hence obtained was then rinsed thoroughly with water and dissolved in 9.3 M LiBr aqueous solution. The solution was then dialyzed in water using a dialysis cassette with a molecular cut off weight of 3500 Da for 48 h. After dialysis, the fibroin solution was transferred into a centrifuge tube. Finally the dialyzed solution was centrifuged for 2 h at 5000 rpm and a temperature of 4º C.

Transmission measurements: Transmission spectra of silk films with and without NDs were measured by placing the samples in close proximity between two optical fiber probes that were coupled to a portable spectrometer. The spectrometer used was *Ocean Optics*, *Dunedin*, *FL*, *USB* 2000 model with a time constant of 100 ms and wavelength in the range 350-1000 nm.

Confocal measurements: Confocal fluorescence scanning was performed using a customized confocal microscope. A 532 nm frequency doubled Nd:YAG continuous wave laser was used to illuminate the sample through a 100 × 0.95 NA objective. The film was mounted on a computer controlled stage equipped with an xyz closed loop positioner with 100 μm travel in each direction and step size resolution of 1 nm. The in-plane optical resolution was approximately 300 nm. Single photon emission was measured with a fiber-based *HBT* interferometer [23], after being filtered with both a 560 nm long pass and 650-750 nm band pass filter. For the non-silk sample, the first confocal scan was used in the manuscript while for the silk-coated-NDs sample, the third successive confocal scan was shown in the manuscript. The emission spectrum of Fig. 1(b) was measured through the same setup but with a filter configuration of 560-850 nm.

FIB markers: The silicon substrate was marked with reference markers, which were prepared by focused ion beam (FIB) milling [22] creating a 2 μm deep pattern. The position of the marker on the substrate was adjusted and measured using a scanning electron microscope.

Silk film deposition on NDs/silicon: The clear water-like silk fibroin solution was drop-casted on top of the NDs/silicon substrate. A 10% volume of silk solution in water was used to create a film with thickness ≈850 nm. The solution crystallized through protein self-assembly upon exposure to air. The cast silk solution was then set to air-dry in a laminar flow hood. The films were then left to dry for 24 h until all the solvent had evaporated to give solid fibroin protein silk film [33, 34].

#197546 - $15.00 USD Received 17 Sep 2013; revised 27 Nov 2013; accepted 12 Dec 2013; published 27 Jan 2014

Animal experiment: The ND-silk films for this step were prepared by mixing ND powder with silk fibroin solution (6% silk fibroin by weight in water) followed by gentle agitation, which gave a uniform silk NDs solution with a concentration of 0.5 mg/mL. The solution was then cast onto a flat hydrophobic substrate (i.e. *PDMS*) and was let dry overnight, resulting in an optically transparent silk ND film with a thickness of 50 μm. The substrate was later peeled off and the as-prepared silk ND film was cut into small pieces of 1 cm × 1 cm, followed by a water annealing process that adjusted the crystallinity level of the silk fibroin films and determined the degradation time of the silk ND films after implantation.

Acknowledgments

P.D. sadly deceased in January 2013, he was supported by an ARC Australian Postdoctoral Fellowship (DP1096831). B.C.G. is supported by an ARC Future Fellowship (FT110100225). S.T-H. is supported by an ARC Australian Research Fellowship (DP1096288).